


Thermal engineering of lead-free nanostructured $\text{CH}_3\text{NH}_3\text{SnCl}_3$ perovskite material for thin-film solar cell

Sk Abdul Moyez · Subhasis Roy 

Received: 25 July 2017 / Accepted: 15 December 2017 / Published online: 30 December 2017
© Springer Science+Business Media B.V., part of Springer Nature 2017

Abstract Perovskite solar cell is a kind of revolutionary investigation in the field of renewable energy which is capable of mitigates the deficiencies of silicon solar cell and its uprising efficiency can bring blessing to society. The presence of lead (Pb) in perovskite solar cell can make worst and negative impact on environment and is not desirable for our society. In this paper, general plans are anticipated by replacement of Pb with tin (Sn) in open atmosphere to fabricate the $\text{CH}_3\text{NH}_3\text{SnCl}_3$ photovoltaic cells in chlorine (Cl)-rich environment. Excess uses of Cl has positive influences on morphological growth of the film and it also suppresses the oxidation tendency of tin (Sn) with existing oxygen in atmosphere and maintains same chemical atmosphere as bulk. Various characterization tools like X-ray diffraction, scanning electron microscope (SEM) have been used to study the effect of annealing temperature on crystal structure, phase formation, impurities, and morphologies of the film. Finally, photovoltaic performance was reported using the solar simulator under 1.5 sun illumination.

Keywords Perovskite · Solar cell · Oxidation · Morphology · Crystalline structure · Energy conversion

S. A. Moyez · S. Roy (✉)
Department of Chemical Engineering, University of Calcutta, 92
A. P. C. Road, Kolkata 700009, India
e-mail: subhasis1093@gmail.com
e-mail: srchemengg@caluniv.ac.in

Introduction

Silicon solar cell is tagged as most effective alternative energy source over the past few decades but an extraordinary new material, called perovskite, poised to completely change the face of the alternative energy sector. The efficient, versatile, inexpensive, light-sensitive perovskite materials have that immense potential to replace all existing alternative energy sources to date. The recent auspicious growth of thin-film organic-inorganic halide hybrid perovskite solar cells, $\text{CH}_3\text{NH}_3\text{PbX}_3$ ($X = \text{I}/\text{Cl}/\text{Br}$) has addressed extensive attention in both scientific and industrial groups, largely owing to the massive power conversion efficiencies (PCE) together with a relatively low cost and scalable processing methods (Nayak and Cahen 2014; Lyu et al. 2016a, b; Lotsch 2014). The elongated carrier diffusion length, a high value of absorption coefficient, direct bandgap properties, and high carrier mobility make this material fittest as solar energy harvester (Stranks et al. 2013; Ananthajothi and Venkatachalam 2016; Dey et al. 2016). Perovskite solar cells have been boosted the power conversion efficiencies from 3.8% at its first appearance in 2009 (Kojima et al. 2009) to more than 20% in recent time (Dey et al. 2017; Green et al. 2014; Kumar et al. 2015; Grätzel 2014; Lee et al. 2012). These organic-inorganic halide hybrid combinations are the member of the ABX_3 perovskite group. Perovskite family makes a structure of material of corner-sharing $(\text{BX}_3)^-$ octahedra, where the B (usually Pb^{2+} or Sn^{2+}) is a divalent metal cation, X (typical halides of Cl^- , Br^- , or I^-) is a monovalent anion; and the monovalent cation

A could be Cs^+ or a minor molecular groups such as methylammonium or formamidinium (Borriello et al. 2008; Lyu et al. 2016a, b; Kagan et al. 1999). Defect-free light-absorbing perovskite thin film with precise grain structure, stable crystalline phase, dense surface coverage, and little to no surface roughness gives the pleasing performance in the crucial area of a coveted perovskite solar cell (Docampo et al. 2013; You et al. 2014; Liang et al. 2014). Perovskite, especially $\text{CH}_3\text{NH}_3\text{PbI}_3$, have already been attended breakthrough efficiency but a serious and hazardous drawback is associated with it, i.e., presence of lead (Pb). Lead poisoning is very baneful and deadly to many organs, and it has a costly impact to the environment (Gidlow 2004). Nontoxic element tin (Sn) is present at the same group in the periodic table with Pb, and it would be exciting to study the effects of substituting Pb in $\text{CH}_3\text{NH}_3\text{PbX}_3$ with Sn. Lead-free organic–inorganic perovskite solar cell's optical, structural, and photovoltaic performances should be comparable with the lead counterpart to achieve efficient solar cell (Hao et al. 2015; Dong et al. 2016). It has been affirmed that the lead-free $\text{CH}_3\text{NH}_3\text{SnI}_3$ could work as a light-harvesting material, and power conversion efficiency in the range of 5–6% have already been achieved (Hao et al. 2015; Moyez et al. 2017). It was reported that lead-free perovskite shows a low PCE due to the instability of the Sn. Sn changes its oxidation state from Sn^{2+} to Sn^{4+} (Moyez et al. 2017) as quickly as come in contact with the ambient oxygen. Poor consistency, defect-effect on crystallinity and non-homogeneous coverage of $\text{CH}_3\text{NH}_3\text{SnI}_3$ film layer are another warning factor which constrains the device performance to a limiting factor (Dong et al. 2016). The reaction rate is recognized to be higher for the SnI_2 and $\text{CH}_3\text{NH}_3\text{I}$ (Sarkar et al. 2017) and it leads to a low-quality film with enormous pin holes (Hao et al. 2014). Though the fabricated film shows less quality, but the density of the carrier for $\text{CH}_3\text{NH}_3\text{SnI}_3$ is larger by one order of magnitude than that of the Pb-based perovskite, $\text{CH}_3\text{NH}_3\text{PbI}_3$, and the recombination lifetime in both cases are equivalent (Hao et al. 2015). In case of $\text{CH}_3\text{NH}_3\text{SnX}_3$, some disordering appears due to the $(\text{CH}_3\text{NH}_3)^+$ cations and distortions of $(\text{SnX}_3)^-$ octahedra at limited annealing temperature (Borriello et al. 2008; Yamamuro et al. 1990; Stoumpos et al. 2013). It was also reported that $\text{CH}_3\text{NH}_3\text{SnX}_3$ exhibits monoclinic and tetragonal phase transitional behavior during low temperature and room temperature, respectively (Dong et al. 2016, Chiarella et al. 2008).

Temperature plays a crucial role as it regulates the crystallinity, crystallite size, crystalline alignment, and the film morphology (Moyez et al. 2016; Roy et al. 2015; Han et al. 2013). The incorporation of chlorine into the $\text{CH}_3\text{NH}_3\text{PbI}_3$ have also been of interest because it increases crystallite size, electron mobility, diffusion length, charge transportation rate, and it decreases the charge recombination rate (Stranks et al. 2013; Edri et al. 2014; Colella et al. 2013; Ball et al. 2013; Mosca et al. 2011).

In this research work, an attempt has been made to replace the hazardous lead (Pb) of the perovskite solar materials by tin (Sn) to fabricate lead-free perovskite solar cell ($\text{CH}_3\text{NH}_3\text{SnCl}_3$), and the effect of annealing temperature (room temperature (30 °C), 70 °C, 80 °C, and 110 °C) on crystal structure has been described. We also studied the structural and optical behavior in presence of excess chlorine (Cl) to suppress the oxidation effects of instable tin (Sn). Interestingly, it was observed that the effects of excess Cl and different annealing temperature have had positive influences on many important parameters. Hence we perform a stimulating research on Cl-based perovskite solar cell with varying annealing temperature at open atmosphere. The influence of the annealing temperature on the film morphology, optical behavior, and structural fundamental and finally photovoltaic device performance were reported systematically.

Experimental

The normal ambient condition was little bit hot and humid during the experiment conducted (temperature 30 °C, relative humidity 70%, wind speed 14 km/h, wind direction south-east facing). Lead-free hybrid perovskite solar cells, $\text{CH}_3\text{NH}_3\text{SnCl}_3$, were prepared at open atmosphere in presence of excess Cl by the following methods:

First, some part of fluorine-doped tin oxide (FTO) glasses were etched by using hydrochloric acid (37% HCl aqueous solutions in H_2O) and Zn powder for making a bottom electrode. This etched FTO-glasses were cleaned using ultra-sonication with adding soap-water, deionized water, acetone, and finally with ethanol for 15 min each. As-prepared titanium nanoparticles sol was used to deposit the thin layer of titanium oxide by spin coating (model spin NXG-P1, Apex Instruments make) at 3000 rpm for 30 s on the top of this cleaned

FTO-glass substrate (15 Ω /cm, Pilkington) followed by the reported literature (Malliga et al. 2014). The coated titanium layer was inserted into furnace and kept at 450 °C for 30 min to the desire TiO₂ phase formation and to remove the organic part. Then, 1.3:1 M ratio of CH₃NH₃Cl and SnCl₂ were dissolved in N,N-dimethylformamide (DMF) organic solvent to prepare CH₃NH₃SnCl₃ solution and the mixture was spin-coated at 3000 rpm for 30 s on the compact TiO₂-coated FTO-glass substrates. This substrate with multilayers coating were annealed at 30 °C, 70 °C, 80 °C, and 110 °C systematically for 60 min followed by copper thiocyanate (CuSCN) deposition as a hole transport materials (HTM) (Zhao et al. 2015). To finish the device fabrication, two contacts were created using an Ag-paste electrode which was applied on the top of the dried multilayers film and bottom of FTO-(etching part) glass. The schematic view of fabricated perovskite solar devices with FTO-glass/TiO₂/CH₃NH₃SnCl₃/HTM/Ag multilayers structure is shown in Fig. 1. Morphological pattern of different films with different annealing condition was evaluated by scanning electron microscopy (SEM). Optical properties were tested under UV-Vis spectrophotometer and structural analysis was evaluated by Rietveld refinement using X-ray diffraction (XRD) data. Finally, current density-voltage characteristics (J-V) were carried out in ambient conditions using a programmable Keithley 2450 source meter under AM 1.5G solar irradiation at 100 mW/cm² using Zolix HPS-300XA light source.

Results and discussion

Scanning electron microscopy

Surface morphology accomplishes an important role on thin film photovoltaic performance. The influence of the annealing temperature on the morphology and structure of the perovskite thin film deposited on FTO-glass had been carried out through SEM. Figure 2 shows the morphology of the CH₃NH₃SnCl₃ films annealed at different temperatures. The growth studies of the lead-free perovskite thin film, CH₃NH₃SnCl₃, as a function of annealing temperature exhibit significant surface morphological changes.

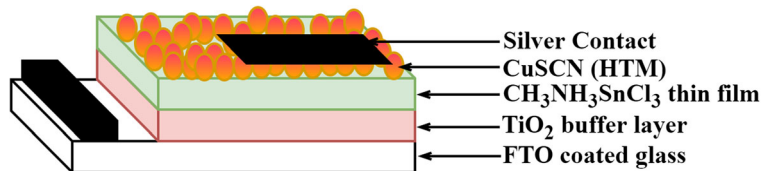
The qualitative morphology pattern of the film prepared at normal room temperature is present in Fig. 2a. It reveals that film has a flowering structure with many

micron-sized rod-like petals are allied with it. It also indicates that the available thermal energy at room temperature driven the nucleation but it is confined to the petal direction only because the thermal energy is more active to that particular direction. The petal growth is almost vertical or perpendicular instead parallel to the substrate surface and hence the big gaps exist in the film. These existing gaps are also exhibiting the incomplete formation of the perovskite from precursor solution due to lack of reaction driven energy. Further increasing annealing temperature to 70 °C brings a vast change immediately on film growth model; especially it enhances the film surface coverage as shown in Fig. 2b. Relatively higher thermal energy at 70 °C has that capability to control the nucleation of the perovskite formation in a wide range but the overall surface is showing a scatter orientation of the leaf with a wide existing gap and many tiny gaps between the leaves. This leaf orientation reveals that initiation of film growth has been stopped after nucleation started from a mid-point of the leaf. This shows that at 70 °C annealing temperature also bearing insufficient thermal energy for the formation of the desirable film and hence discontinuity and an enormous number of a sleazy channel created in the film. Drastic changes appeared on the surface morphology as the annealing temperature reaches at 80 °C (see Fig. 2c). The perovskite film formed square nanoparticles in the range of 30–40 nm over the whole surface. The underneath of the square nanoparticles are full of the homogenous thin layer of desired perovskite materials (see “X-ray diffraction” also). It was also observed that the high heat energy at 80 °C leads the precursor solution towards establishing a complete reaction; hence, the high annealing energy helps to form the comparable higher quality, dense film. Upon annealing at 110 °C, the film changed its nature to piecrust flake-like structure as shown in Fig. 2d. This film has inhomogeneous morphology even though the film formed at higher thermal energy due to thermal molecular diffusion.

X-ray diffraction

The phase analysis of the synthesized CH₃NH₃SnCl₃ alone was carried out using a rapid analytical technique, X-ray diffraction (XRD) tool [model Miniflex-ZD06184, Rigaku make], equipped with a graphite monochromator with Cu K α (λ = 1.54 Å). The obtained experimental X-ray diffraction profiles of CH₃NH₃SnCl₃ are presented in Fig. 3. The experimental XRD data were

Fig. 1 Schematic view of fabricated perovskite solar devices



analyzed with standard XRD profile using Rietveld refinement to confirm the purity of $\text{CH}_3\text{NH}_3\text{SnCl}_3$ phase. Figure 3a shows the presence of extra peaks at 11.80 and 24.27 (2θ) degree which are $\text{SnCl}_3(\text{OH})(\text{H}_2\text{O})$ and SnO_2 , respectively. It stating that lower thermal energy for the film fabricated at room temperature, 30 °C, is unable to drive the precursor liquid completely from the thin film to form perovskite-rich solid uniform thin film due to lack of sufficient thermal energy at room temperature. The unstable Sn oxidized with the oxygen present in the air easily and unwanted SnCl_2 hydrated with the air moisture. This kind of phenomenon indicates the insufficient thermal energy, at room temperature, is unable to vaporize the precursor liquid completely and incomplete nucleation constraints the desired perovskite phase formation.

It was observed that further heating beyond the room temperature i.e., at 70, 80, and 110 °C is quite able to dry the solid film completely to form the pure perovskite phase $\text{CH}_3\text{NH}_3\text{SnCl}_3$ as reported earlier (Hao et al. 2015; Ogomi et al. 2014). High thermal energy at 70, 80, and 110 °C leads to grow pure and complete perovskite formation which is the evidence by peaks formation at 15.46, 31.40, and 47.9 (2θ) degree. The newly

appear peak at 31.40 (2θ) degree has higher intensity for the film annealed at 80 °C compare to the 70 and 110 °C. The reason behind the higher intensity at 80 °C is due to crystallite size and their crystalline structure orientation. The refinement study clearly indicates that different annealing temperature has crucial influences on the crystal formation of $\text{CH}_3\text{NH}_3\text{SnCl}_3$ because thermal energy is the only external influencing factor which is affecting the crystalline system of the $\text{CH}_3\text{NH}_3\text{SnCl}_3$ at their atomic level. Figure 4 depicts the orientation of crystalline system based on their annealing temperature. The role of the annealing temperature is to vaporize the organic liquid from the precursor solution and monitoring the controllable growth of the perovskite phases in the solid film. MASnX_3 (X = I, Cl, and Br) exhibit phase transition tendency as a function of temperature already reported before (Chiarella et al. 2008; Roiati et al. 2014). It may notice that the $\text{CH}_3\text{NH}_3\text{SnCl}_3$ changes its crystalline structure from triclinic to rhombohedral with increasing annealing temperature from room temperature to 110 °C. The less symmetric triclinic crystalline structure is formed at lower temperature due to insufficient thermal energy. The triclinic crystalline structure reorganized to the

Fig. 2 SEM images of $\text{CH}_3\text{NH}_3\text{SnCl}_3$ thin films at different annealing temperature at **a** 30 °C (room temperature), **b** 70 °C, **c** 80 °C, and **d** 110 °C

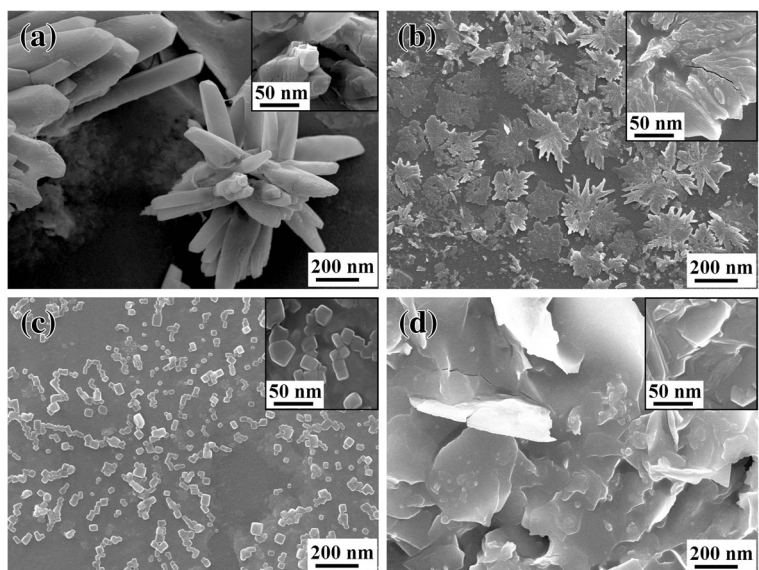
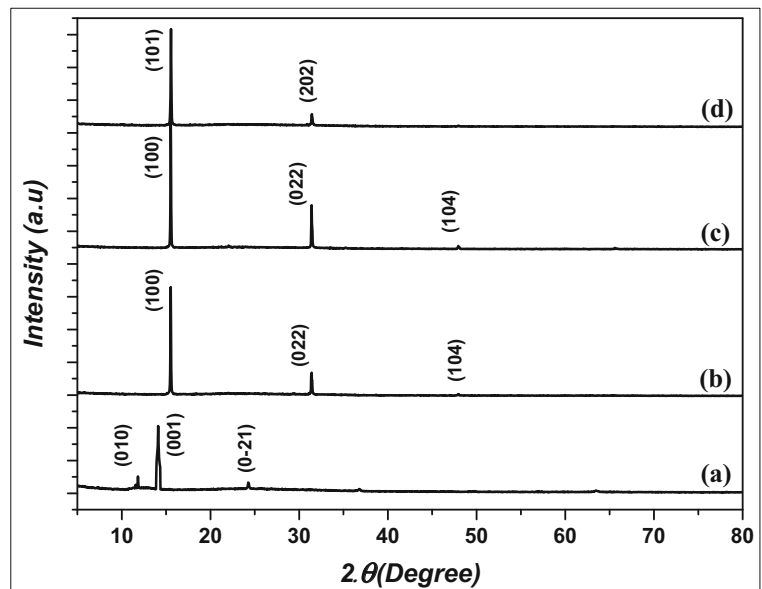


Fig. 3 X-ray diffraction of $\text{CH}_3\text{NH}_3\text{SnCl}_3$ thin films treated with different annealing temperature at (a) room temperature 30 °C, (b) 70 °C, (c) 80 °C, and (d) 110 °C

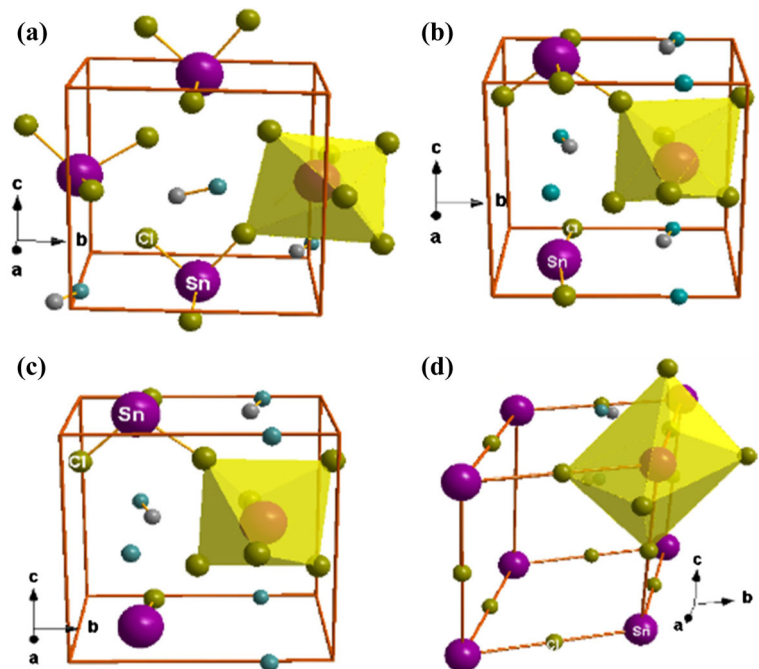


monoclinic structure at 70 and 80 °C annealing temperature but the much higher temperature at 110 °C established a rhombohedral structure. This reorganizing crystal structure transformation indicates that the low temperature is not sufficient to vaporize the precursor liquid and accelerate the complete nucleation properly; hence, a little amount of residual stress remains presents in the crystalline structure. The remaining residual stress creates a crystalline depression (internal stress) in the structure and the depressed crystalline perovskite structure finds a way to achieve a better symmetry. The crystalline depression or the present residual stress is suppressed with increasing temperature to the 70, 80, or 110 °C and a better crystalline stability achieved. But further increments of the temperature beyond the 80 °C, at 110 °C, have had an adverse effect on crystalline stability due to an octahedral distortions of $(\text{SnCl}_3)^-$ and disordered arrangement of $(\text{CH}_3\text{NH}_3)^+$ cations which are the primary responsible for the phase transitional activities of $\text{CH}_3\text{NH}_3\text{SnCl}_3$. A symmetrical orientation occurs for the $(\text{SnCl}_3)^-$ octahedral unit in case of the high-temperature rhombohedral phase heated at 110 °C which makes a complete disorder orientation of the $(\text{CH}_3\text{NH}_3)^+$ cations. This disordered orientation of the $(\text{CH}_3\text{NH}_3)^+$ creates an internal inhomogeneous jerking in the crystalline structure. Due to the distorted structural formation and crystalline disturbance the 104 peak of $\text{CH}_3\text{NH}_3\text{SnCl}_3$ at 47.9 (2θ) degree is missing for 110 °C annealing film. At 70 or 80 °C fabrication temperature, the $(\text{SnCl}_3)^-$ octahedral lost its symmetrical

orientation (Fig. 5) and a regional potential barrier build against the $(\text{CH}_3\text{NH}_3)^+$ cation because of tilting and distortion of the $(\text{SnCl}_3)^-$ octahedral which destroying the disorder orientation of $(\text{CH}_3\text{NH}_3)^+$ cations and release the unwanted crystalline depression (residual stress). Accordingly, the lower symmetry $\text{CH}_3\text{NH}_3\text{SnCl}_3$ crystalline structures, formed at 70 and 80 °C compared to the 110 °C, have more ordered orientation, stable crystalline structure and systematic order of $(\text{CH}_3\text{NH}_3)^+$ cations.

Experimentally, extracted lattice parameters of 70 and 80 °C in Table 1 are clearly indicating that the unit cell formed at the 80 °C has shrinkage in the “a” direction (6.5%) an obvious expanding tendency occurs in the “b,” and “c” directions. The unit cell formed at 80 °C releases its existed excessive residual stress or crystalline depression towards the “a” lattice direction and at the same time a distortion of the $(\text{SnCl}_3)^-$ octahedral started to produce due to shrinkage of the “a” which weakens the disordered arrangement of the $(\text{CH}_3\text{NH}_3)^+$ cations. The monoclinic crystalline structure at 80 °C compare to the 70 °C achieved more symmetrical orientation by releasing the excess residual stresses (or crystalline depression) and $(\text{CH}_3\text{NH}_3)^+$ cations fitted best at its convenient position. Nevertheless, the same theory could not be applied for all cases in this experiment because different crystalline structure formation happens for others case. So, this conclusion could be drawn exclusively from these two cases only since both systems have the same crystalline structure.

Fig. 4 Different crystalline structure formation of the $\text{CH}_3\text{NH}_3\text{SnCl}_3$ at **a** 30 °C (room temperature), **b** 70 °C, **c** 80 °C, and **d** 110 °C



Tin (Sn) also plays another important role beside the orientation of the $(\text{CH}_3\text{NH}_3)^+$ cations and $(\text{SnCl}_3)^-$ octahedra. Sn^{+2} gets easily oxidized to the Sn^{+4} with existing oxygen in the open environment. Especially the Sn present at the surface gets easily affected in this

junction. So a rigorous controlling of oxygen is required to defend the oxidation tendency of Sn for which the surface of the thin film is unable to form $(\text{SnCl}_3)^-$ octahedral due to insufficient Cl present; hence, a Cl-rich environment is required to suppress the oxidation

Fig. 5 Orientation of the crystal structure (unit cell) at 100 direction of the film fabricated at (a₁₀₀) 30 °C (room temperature), (b₁₀₀) 70 °C, (c₁₀₀) 80 °C, and (d₁₀₀) 110 °C. The figure indicating the orientation of the $(\text{SnCl}_3)^-$ octahedral and $(\text{CH}_3\text{NH}_3)^+$ cations

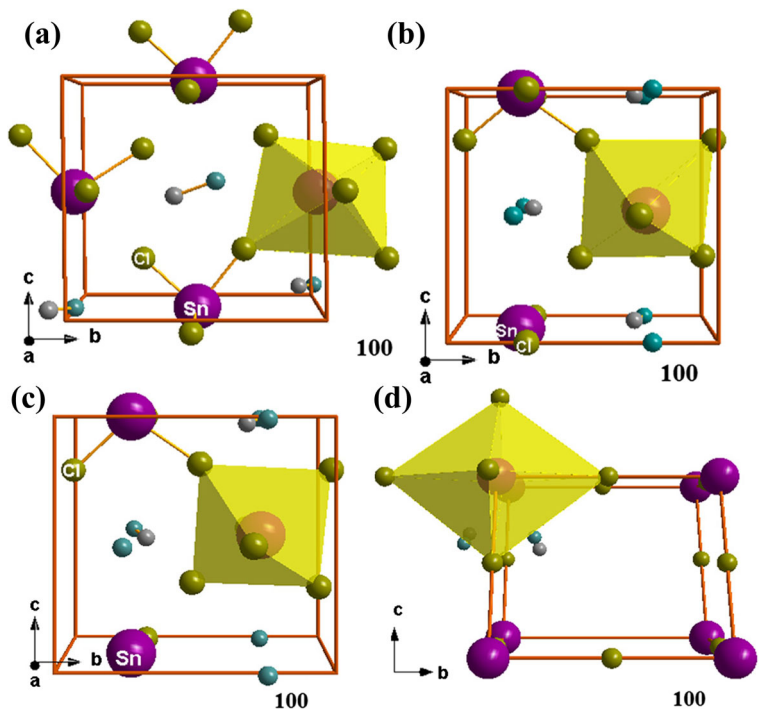


Table 1 Extracted data of lattice parameters after refinement of CH₃NH₃SnCl₃ perovskite materials annealed at different temperatures

Annealed temperature	a (Å)	b (Å)	c (Å)	α (°)	β (°)	γ (°)	Cell vol. (Å ³)	Crystal structure
Room temp	5.781	8.133	7.849	90.82	93.18	89.98	369.04	Triclinic
70 °C	5.720	8.064	7.690	90	92.94	90	354.71	Monoclinic
80 °C	5.346	8.357	7.871	90	91.17	90	351.65	Monoclinic
110 °C	8.365	8.365	9.185	90	90	120	642.70	Rhombohedral

effect of the Sn. Maintaining the excess Cl-ion environment, the surface-Sn form the desire (SnCl₃)⁻ octahedral and an inert chemical environment established same environment as the bulk CH₃NH₃SnCl₃ (Yin et al. 2014; Frost et al. 2014).

The previous study reported that the fundamental bandgap and volume of the unit cell of the hybrid perovskite solar cell are directly proportional (Frost et al. 2014; Feng and Xiao 2014). In this experiment, the unit cell volume of the film fabricated at 80 °C, 70 °C, room temperature, and 110 °C have ascending order (Table 1) and the experimental bandgap also obeyed this ascending manner which is fully satisfied the previous work (Feng and Xiao 2014). The achieved lower bandgap value for the film fabricate at 80 °C has had a positive role beside the higher crystalline stability towards the formation of the CH₃NH₃SnCl₃ perovskite photovoltaic.

Ultraviolet-visible spectroscopy

Absorbance and absorption coefficient

The in-depth analysis of the UV-visible spectroscopy especially the absorbance, reveals the light interaction

fundamental, light absorbing behavior and unlocks some basic outline of semiconducting properties of a photovoltaic material. Absorption coefficient (α) describes the light absorbing strength of a material by the given Kubelka-Munk, Eq. 1,

$$\alpha = \frac{(1-R)^2}{2R} \tag{1}$$

where *R* is the reflected percentage of light and α is the absorption coefficients. From UV-Vis spectroscopy, a primary conclusion about a material’s applicability in the photovoltaic system could easily be drawn. Figure 6a represents the absorbance plot against the wavelength, and Fig. 6b describes the corresponding absorption coefficient with respect to the photon energy of these perovskite multilayer films under at different annealing conditions. These figures show that extremely low absorbing tendency occurs for the film prepared at room temperature (30 °C) due to phase impurities and incomplete conversion of CH₃NH₃SnCl₃ from precursor solution. The corresponding absorption coefficient value (α), Fig. 6b, indicates extremely low absorption coefficient in the order of 10³ cm⁻¹ (Table 2) for the film prepared at room temperature due to less interaction of light with the film. In the case of high annealing

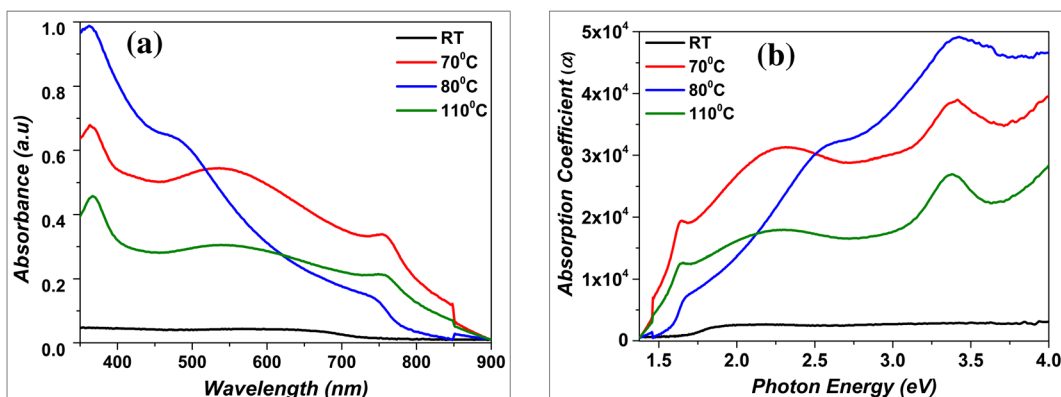


Fig. 6 Optical properties for CH₃NH₃SnCl₃ perovskite thin films at different annealing condition. **a** The absorbance vs wavelength (nm) spectra and **b** variation of optical absorption coefficient α(λ) as a function of wavelength (nm)

Table 2 Value of the absorption coefficient (α), direct bandgap energy (E_g), Urbach energy (E_U), and the constant (α_0) are extracted from the UV-visible spectroscopy

Annealing temp. (°C)	α (maximum) (cm^{-1})	Bandgap, E_g (eV)	Urbach energy, E_U (meV)	The constant (α_0) (cm^{-1})
Room temperature	2.9×10^3	2.30	250	90
70 °C	38×10^4	2.18	67	121
80 °C	49×10^4	2.15	64	148
110 °C	26×10^4	2.70	80	74

temperature at 70, 80, and 110 °C, a handy improvement in absorbance and absorption coefficient, in the order of 10^4 cm^{-1} , was found which could be well fitted for photovoltaic and others photonic application. The peak value of the optical parameters was achieved at 80 °C but the further increment of annealing temperature to 110 °C shows a declining tendency on both absorbance and absorption coefficient (α). Highest degree of absorption and large absorption coefficient value, α , in the order of 10^4 cm^{-1} (Table 2), was found at 80 °C. Decent optimized optical properties have occurred across the entire spectral range for the film annealed at 80 °C compared to the film fabricated at room temperature, 70, and 110 °C due to highly oriented, smooth and well-organized film with fewer defects. This optical phenomenon reveals that different annealing temperature plays a crucial role for the formation of desired light sensing $\text{CH}_3\text{NH}_3\text{SnCl}_3$ perovskite material. At room temperature and 70 °C, the partial formation of $\text{CH}_3\text{NH}_3\text{SnCl}_3$ perovskite occurred and hence, wild grain gaps and defects are present in these films due to improper phase formation which supports the SEM analysis (Fig. 2). Excess SnCl_2 and CH_3NH_3^+ may also remain after the

film annealing at room temperature due to insufficient thermal energy. Figure 6 indicates that the absorbance is quite low for the film annealed at 110 °C because of the less symmetrical crystalline formation and high residual stress present which is already discussed in the XRD part. It may also be concluded that the high annealing energy has had an adverse effect on the $\text{CH}_3\text{NH}_3\text{SnCl}_3$ thin film formation as the high heat energy leads to the instability of the $\text{CH}_3\text{NH}_3\text{SnCl}_3$ materials. It is obvious from the figure that the film annealed at 80 °C has a better aspect in terms of light absorbing tendency. In this experiment, a little absorption edge appeared between 1.6 and 2.5 eV due to the presence of excess CH_3NH_3^+ at the dried film because of the higher amount of $\text{CH}_3\text{NH}_3\text{Cl}$ used to maintain a Cl-rich environment, and it will not hamper the energy band calculation of the perovskite film anymore.

Urbach energy

The Urbach Energy, E_U , reflects the presence of defects, disorders, impurities, and portrays the crystallinity nature of the thin film. The E_U can be investigated from

Fig. 7 $\ln(\alpha)$ vs photon energy (eV) of the lead-free, $\text{CH}_3\text{NH}_3\text{SnCl}_3$, perovskite solar material, prepared under various annealing temperature

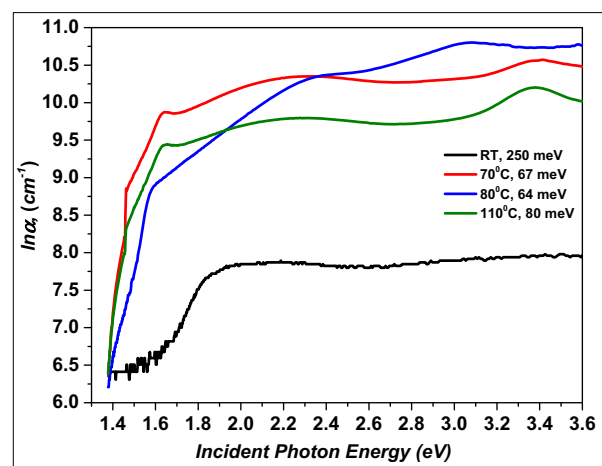
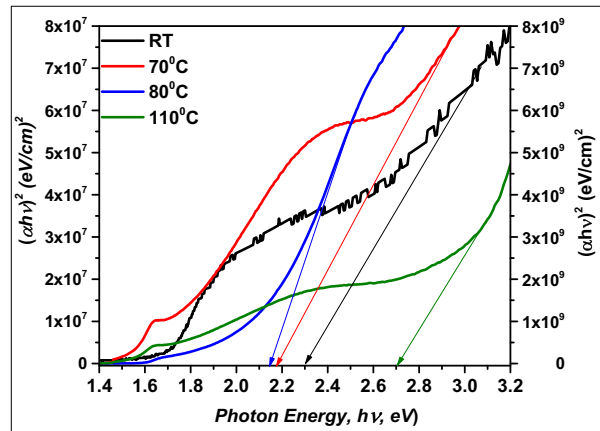


Fig. 8 The bandgap energy determination of the $\text{CH}_3\text{NH}_3\text{SnCl}_3$ perovskite film fabricated at room temperature, 70, 80, and 110 °C



absorption spectra, and the width of the exponential tail increases according to the density of defects and disorders. E_U can be calculated from the inversion of the slope of the tail part by plotting $\ln(\alpha)$ against the photon energy ($h\nu$) from the following Eqs. 2 and 3.

$$\alpha = \alpha_0 \exp \frac{h\nu}{E_U} \tag{2}$$

$$\ln(\alpha) = \ln(\alpha_0) + \frac{h\nu}{E_U} \tag{3}$$

where α_0 is a constant and E_U is called Urbach energy, $h\nu$ is the photon energy.

The E_U values of the annealed $\text{CH}_3\text{NH}_3\text{SnCl}_3$ films at 30, 70, 80, and 110 °C, calculated from the tail part of Fig. 7, are 250, 67, 64, and 80 meV, respectively. Though these experimental values are slightly higher than that of

reported E_U (15 meV for $\text{CH}_3\text{NH}_3\text{PbI}_3$) [25], nevertheless, it has some great significance since the films were fabricated at the open environment. The higher E_U at room temperature, 70, and 110 °C compare to the 80 °C has been indicating that there may be higher degree of defect presents in these films. The E_U values signify that thermal energy at 80 °C maintains a smooth and homogeneous nucleation throughout the whole film, but on the other side, an inhomogeneous nucleation occurs for the film fabricated at room temperature, 70, and 110 °C.

Optical energy gap determination

Perovskite materials, especially ABX_3 ($A = \text{CH}_3\text{NH}_3/\text{Cs}$, $B = \text{Pb}/\text{Sn}$, $X = \text{I}/\text{Cl}/\text{Br}$), could efficiently be used as photovoltaic since it has the bandgap in the range of 1.5

Fig. 9 J-V characterization of $\text{CH}_3\text{NH}_3\text{SnCl}_3$ carried out under AM 1.5G illuminations (100 mW cm^{-2})

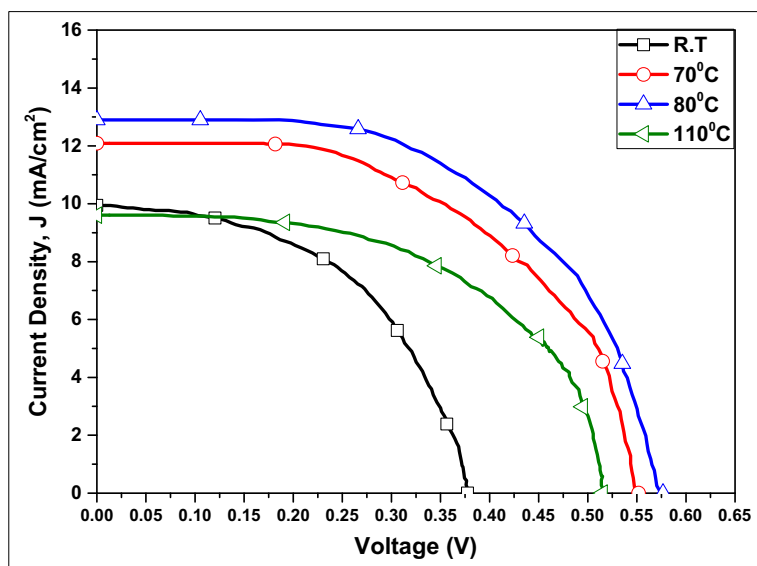


Table 3 Photovoltaic parameters generated from J-V characterization. The illuminated areas of all devices were 1.2 cm²

Annealing temperature	V_{OC} (mV)	J_{SC} (mA cm ⁻²)	P_{max}	FF	Efficiency (%)
Room temperature	377	9.94	1.93	0.51	1.61
70 °C	551	12.09	3.59	0.53	3.00
80 °C	576	12.89	4.10	0.55	3.41
110 °C	515	9.60	2.76	0.55	2.30

to 3.5 eV. The bandgap of the CH₃NH₃SnCl₃ could easily be calculated by following Tauc's relationship, Eq. 4, using the optical absorption data.

$$\alpha h\nu = \alpha_0(h\nu - E_g)^n \quad (4)$$

where α_0 is a constant, and E_g is the optical energy gap or bandgap. $n = 1/2$ in case of direct allowed so the Eq. 4 turns to Eq. 5 for perovskite materials.

$$(\alpha h\nu)^2 = \alpha_0(h\nu - E_g) \quad (5)$$

It is necessary to plot $(\alpha h\nu)^2$ versus against photon energy ($h\nu$) to determine the energy bandgap value from the experimental optical absorption data, as shown in Fig. 8 and Table 2, and prolong the existing straight line up to $(\alpha h\nu)^2 = 0$ to $h\nu$ axis. The experimentally extracted bandgap values, from Fig. 8, are lowering with temperature enhancement up to 80 °C but it suddenly enhanced at 110 °C temperature. The film fabricated at 80 °C is capable of absorbing higher amount of visible spectrum than the rest of the cases and it generates higher amount of photo exciton carrier.

Photovoltaic performance

The current density-voltage (J-V) measurement of CH₃NH₃SnCl₃ was carried on 1.2 cm² active device area for each case under AM 1.5G standard illumination, using Keithley 2450 source meter and Zolix light source of 100 mWcm⁻², are presented in Fig. 9 and the equivalent data are furnished in Table 3. The device annealed at 80 °C generates the maximum power conversion efficiency (PCE), 3.41%, with maximum open-circuit voltage (V_{OC}) of 576 mV, and highest short-current density (J_{SC}), 12.89 mA cm⁻² whereas the device fabricated at room temperature, 70, and 110 °C are comparatively less efficient. They generates 1.61, 3.00, and 2.30% efficiency along with 377, 551, and 515 mV open-circuit voltage (V_{OC}) and 9.94 mA cm⁻², 12.09 mA cm⁻², and 9.60 mA cm⁻² short circuit current

density (J_{SC}), respectively. Incomplete perovskite conversion occurs for the device fabricated at room temperature leads to minimum efficiency. The extracted efficiency of CH₃NH₃SnCl₃ exhibiting a reverse tendency with annealing temperature up to 80 °C from room temperature and an efficiency dropping occurs for 110 °C. This tendency can be described by the wider bandgap formation, scattered morphological orientation, and higher amount of residual stress present at high temperatures, at 110 °C, which is well fitted with UV-vis and the XRD measurements data, respectively. The film fabricated at 80 °C has nano-square formation which exposed and absorb more photon energy and capable of producing the higher amount of excitons, as the nanoparticle has the highest surface to volume ratio, which generates higher efficiency. The presence of more objectionable exciton trapping states hampering the device performance and device quality for the film fabricated at room temperature, 70 °C, and it shows less performance than the film annealed at 80 °C. The fill factor (FF) of the device prepared at room temperature 70, 80, and 110 °C, are 0.51, 0.53, 0.55, and 0.55, respectively.

Conclusion

The present work focused on improving the performance of the lead-free CH₃NH₃SnCl₃ perovskite to fabricate the highly efficient photovoltaic device by reducing the defect density, crystalline depression, and instability of Sn. In this experiment, we have explored the critical impact of annealing temperature on the optical properties, surface morphology, and structural behaviors of lead-free perovskite CH₃NH₃SnCl₃, which was synthesized by the one-step method from precursor solution of SnCl₂ and CH₃NH₃Cl (1:1.3 M ratio) in DMF solvent. The influences observed by annealing temperatures on crystalline structure, optical behavior, and morphology have a clear correlation with photovoltaic performance. Surface morphology study, structural

behavior, optical analysis, and photo conversion efficiency suggests that 80 °C is the optimized and satisfactory temperature to assemble the $\text{CH}_3\text{NH}_3\text{SnCl}_3$ perovskite-based photovoltaic device. The insufficient thermal energy at room temperature leads to incomplete perovskite conversion and incomplete nucleation which constrain the undesired light-harvesting perovskite phase formation. An improper morphology constructed at room temperature due to the lower thermal energy produces more recombination states where the exciton get neutralized, and it is unable to generate satisfactory exciton. The film fabricated at 70 °C annealing temperature has photovoltaic performance marginally lower than 80 °C because of more defects, higher recombination centers, slightly higher bandgap (E_g), and large crystalline depression (residual stress). It was observed that the device quality enhanced with increasing thermal energy up to 80 °C and again the performance dropped beyond that temperature, at 110 °C. The film annealed at 80 °C has less-distorted and well-balanced crystallized structure with well-organized nano-square rich morphology which shows the highest absorbance with less defects leading to the high-performance photovoltaic device. But at higher temperature more than 80 °C, device quality degrades which affects the device performances. At higher annealing temperature, for 110 °C, the crystalline instability increases due to higher distortion and internal stress, enhancement of bandgap (E_g), and defects in film surface. This blending effect brought an overmuch reduction in film quality which limited its overall photovoltaic performance.

Acknowledgements We would like to thank Dr. Asit Baran Biswas, Assistant professor, Department of Chemical Engineering, University of Calcutta for providing valuable suggestions.

Funding Information This work is supported by Science and Engineering Research Board (SERB), grants funded by Department of Science and Technology (DST), Central Government of India through Fast Track Scheme for Young Scientists (Registration no. 175/2013, SB/FT/CS-105/2013) and University Grand Commission (UGC), India through Maulana Azad National Fellowship (Award letter no. F1-17.1/2014-15/MANF-2014-15-MUS-WES-47983).

Compliance with ethical standards

Conflict of interest Author SR has received research grants from Science and Engineering Research Board (SERB) funded by Department of Science and Technology (DST), Central Government of India through Fast Track Scheme for Young Scientists (Registration no. 175/2013, SB/FT/CS-105/2013 and Author Sk.

AM received Maulana Azad National Fellowship (Award letter no. F1-17.1/2014-15/MANF-2014-15-MUS-WES-47983).

References

- Ananthajothi P, Venkatachalam P (2016) Tin chloride perovskite-sensitized core/shell photoanode solar cell with spiro-MeOTAD hole transport material for enhanced solar light harvesting. *J Solid State Electrochem* 20(10):2633–2642. <https://doi.org/10.1007/s10008-016-3262-z>
- Ball JM, Lee MM, Hey A, Snaith HJ (2013) Low-temperature processed meso-superstructured to thin-film perovskite solar cells. *Energy Environ Sci* 6(6):1739–1743. <https://doi.org/10.1039/c3ee40810h>
- Borriello I, Cantele G, Ninno D (2008) Ab initio investigation of hybrid organic-inorganic perovskites based on tin halides. *Phys Rev B* 77(23):235214. <https://doi.org/10.1103/PhysRevB.77.235214>
- Chiarella F, Zappettini A, Licci F, Borriello I, Cantele G, Ninno D, Cassinese A, Vaglio R (2008) Combined experimental and theoretical investigation of optical, structural, and electronic properties of $\text{CH}_3\text{NH}_3\text{SnX}_3$ thin films. (X=Cl,Br). *Phys Rev B* 77:0451294
- Colella S, Mosconi E, Fedeli P, Listorti A, Gazza F, Orlandi F, Ferro P, Besagni T, Rizzo A, Calestani G (2013) $\text{MAPbI}_{3-x}\text{Cl}_x$ mixed halide perovskite for hybrid solar cells: the role of chloride as dopant on the transport and structural properties. *Chem Mater* 25(22):4613–4618. <https://doi.org/10.1021/cm402919x>
- Dey A, Moyez A, Mandal MK, Roy S (2016) Fabrication of solar cell using extracted biomolecules from tea leaves and hybrid perovskites. *Mat Today Proc* 3:3498–3504
- Dey A, Karan P, Sengupta A, Moyez SA, Sarkar P, Majumder SB, Pradhan D, Roy S (2017) Enhanced charge carrier generation by dielectric nanomaterials for quantum dots solar cells based on CdS-TiO₂ photoanode. *Sol Energy* 158:83–88. <https://doi.org/10.1016/j.solener.2017.09.038>
- Docampo P, Ball JM, Darwich M, Eperon GE, Snaith HJ (2013) Efficient organometal trihalide perovskite planar-heterojunction solar cells on flexible polymer substrates. *Nat Commun* 4:2761–2766
- Dong X, Fang X, Lv M, Lin B, Zhang S, Wang Y, Yuan N, Ding J (2016) Method for improving illumination instability of organic-inorganic halide perovskite solar cells. *Sci Bull* 61(3):236–244. <https://doi.org/10.1007/s11434-016-0994-1>
- Edri E, Kirmayer S, Kulbak M, Hodes G, Cahen D (2014) Chloride inclusion and hole transport material doping to improve methyl ammonium lead bromide perovskite-based high open-circuit voltage solar cells. *J Phys Chem Lett* 5(3):429–433. <https://doi.org/10.1021/jz402706q>
- Feng J, Xiao B (2014) Effective masses and electronic and optical properties of nontoxic MASnX_3 (X=Cl, Br, and I) perovskite structures as solar cell absorber: a theoretical study using HSE06. *J Phys Chem C* 118(34):19655–19660. <https://doi.org/10.1021/jp506498k>
- Frost JM, Butler KT, Brivio F, Hendon CH, van Schilfgaarde M, Walsh A (2014) Atomistic origins of high-performance in

- hybrid halide perovskite solar cells. *Nano Lett* 14(5):2584–2590. <https://doi.org/10.1021/nl500390f>
- Gidlow DA (2004) Lead toxicity. *Occup Med (Lond)* 54(2):76–81. <https://doi.org/10.1093/occmed/kqh019>
- Grätzel M (2014) The light and shade of perovskite solar cells. *Nat Mater* 13(9):838–842. <https://doi.org/10.1038/nmat4065>
- Green MA, Ho-Baillie A, Snaith HJ (2014) The emergence of perovskite solar cells. *Nat Photon* 8(7):506–514. <https://doi.org/10.1038/nphoton.2014.134>
- Han GS, Lee S, Kim DW, Kim DH, Noh JH, Park JH, Roy S, Ahn TK (2013) A simple method to control morphology of hydroxyapatite nano-and microcrystals by altering phase transition route. *Cryst Growth Des* 13(8):3414–3418. <https://doi.org/10.1021/cg400308a>
- Hao F, Stoumpos CC, Chang RPH, Kanatzidis MG (2014) Anomalous band gap behavior in mixed Sn and Pb perovskites enables broadening of absorption spectrum in solar cells. *J Am Chem Soc* 136(22):8094–8099. <https://doi.org/10.1021/ja5033259>
- Hao F, Stoumpos CC, Guo P, Zhou N, Marks TJ, Chang RPH, Kanatzidis MG (2015) Solvent-mediated crystallization of $\text{CH}_3\text{NH}_3\text{SnI}_3$ films for heterojunction depleted perovskite solar cells. *J Am Chem Soc* 137(35):11445–11452. <https://doi.org/10.1021/jacs.5b06658>
- Kagan CR, Mitzi DB, Dimitrakopoulos CD (1999) Organic-inorganic hybrid materials as semiconducting channels in thin-film field-effect transistors. *Science* 286(5441):945–947. <https://doi.org/10.1126/science.286.5441.945>
- Kojima A, Teshima K, Shirai Y, Miyasaka T (2009) Organometal halide perovskites as visible-light sensitizers for photovoltaic cells. *J Am Chem Soc* 131(17):6050–6051. <https://doi.org/10.1021/ja809598r>
- Kumar MH, Dharani S, Leong WL, Boix PP, Prabhakar RR, Baikie T, Shi C, Ding H, Ramesh R, Asta M, Graetzel M, Mhaisalkar SG, Mathews N (2015) Lead-free halide perovskite solar cells with high photocurrents realized through vacancy modulation. *Adv Mater* 26(41):7122–7127
- Lee MM, Teuscher J, Miyasaka T, Murakami TN, Snaith HJ (2012) Efficient hybrid solar cells based on meso-structured organometal halide perovskites. *Science* 338(6107):643–647. <https://doi.org/10.1126/science.1228604>
- Liang PW, Liao CY, Chueh CC, Zuo F, Williams ST, Xin XK, Lin J, Jen AKY (2014) Additive enhanced crystallization of solution-processed perovskite for highly efficient planar-heterojunction solar cells. *Adv Mater* 26(22):3748–3754. <https://doi.org/10.1002/adma.201400231>
- Lotsch BV (2014) New light on an old story: perovskites go solar. *Angew Chem Int Ed* 53(3):635–637. <https://doi.org/10.1002/anie.201309368>
- Lyu M, Yun JH, Cai M, Jiao Y, Bernhardt PV, Zhang M, Wang Q, Du A, Wang H, Liu G, Wang L (2016a) Organic-inorganic bismuth (III)-based material: a lead-free, air-stable and solution-processable light-absorber beyond organolead perovskites. *Nano Res* 9(3):692–702. <https://doi.org/10.1007/s12274-015-0948-y>
- Lyu M, Zhang M, Cooling NA, Jiao Y, Wang Q, Yun JH, Vaughan B, Triani G, Evans P, Zhou X, Feron K, Du A, Dastoor P, Wang L (2016b) Highly compact and uniform $\text{CH}_3\text{NH}_3\text{Sn}_{0.5}\text{Pb}_{0.5}\text{I}_3$ films for efficient panchromatic planar perovskite solar cells. *Sci Bull* 61(20):1558–1562. <https://doi.org/10.1007/s11434-016-1147-2>
- Malliga P, Pandiarajan J, Prithivikumaran N, Neyvasagam K (2014) Influence of film thickness on structural and optical properties of sol-gel spin coated TiO_2 thin film. *IOSR-JAP* 6(1):22–28. <https://doi.org/10.9790/4861-06112228>
- Mosca R, Ferro P, Besagni T, Calestani D, Chiarella F, Licci F (2011) Effect of humidity on the a.c. impedance of $\text{CH}_3\text{NH}_3\text{SnCl}_3$ hybrid films. *Appl Phys A Mater Sci Process* 104(4):1181–1187. <https://doi.org/10.1007/s00339-011-6407-z>
- Moyez A, Dhar A, Sarkar P, Jung HS, Roy S (2016) A review of the multiple exciton generation in photovoltaics. *Rev Adv Sci Eng* 5(1):51–64. <https://doi.org/10.1166/rase.2016.1108>
- Moyez SA, Sengupta A, Biswas AB, Roy S, Dey A, Das BC (2017) Fabrication of environmental friendly perovskite solar cell by partial replacement of lead with tin. *Invertis J Renew Energy* 7(2):59–63
- Nayak PK, Cahen D (2014) Updated assessment of possibilities and limits for solar cells. *Adv Mater* 26(10):1622–1628. <https://doi.org/10.1002/adma.201304620>
- Ogomi Y, Morita A, Tsukamoto S, Saitho T, Fujikawa N, Shen Q, Toyoda T, Yoshino K, Pandey SS, Ma T, Hayase S (2014) $\text{CH}_3\text{NH}_3\text{Sn}_x\text{Pb}_{(1-x)}\text{I}_3$ perovskite solar cells covering up to 1060 nm. *J Phys Chem Lett* 5(6):1004–1011. <https://doi.org/10.1021/jz5002117>
- Roiati V, Mosconi E, Listorti A, Colella S, Gigli G, De Angelis F (2014) Stark effect in perovskite/ TiO_2 solar cells: evidence of local interfacial order. *Nano Lett* 14(4):2168–2174. <https://doi.org/10.1021/nl500544c>
- Roy S, Han GS, Shin H, Lee JW, Mun J, Shin H, Jung HS (2015) Low temperature synthesis of rutile TiO_2 nanocrystals and their photovoltaic and photocatalytic properties. *J Nanosci Nanotechnol* 15:4516–4521
- Sarkar P, Moyez SA, Dey A, Roy S, Das SK (2017) Experimental investigation of photocatalytic and photovoltaic activity of titania/rice husk crystalline nano-silica hybrid composite. *Sol Energy Mater Sol* 172:93–98. <https://doi.org/10.1016/j.solmat.2017.07.021>
- Stoumpos CC, Malliakas CD, Kanatzidis MG (2013) Semiconducting tin and lead iodide perovskites with organic cations: phase transitions, high mobilities, and near-infrared photoluminescent properties. *Inorg Chem* 52(15):9019–9038. <https://doi.org/10.1021/ic401215x>
- Stranks SD, Eperon GE, Grancini G, Menelaou C, Alcocer MJP, Leijtens T, Herz LM, Petrozza A, Snaith HJ (2013) Electron-hole diffusion lengths exceeding 1 micrometer in an organometal trihalide perovskite absorber. *Science* 342(6156):341–344. <https://doi.org/10.1126/science.1243982>
- Yamamoto NO, Matsuo T, Suga H (1990) Calorimetric and IR spectroscopy studies of phase transitions in methylammonium trihalogenoplumbates (ii). *J Phys Chem Solids* 51(12):1383–1395. [https://doi.org/10.1016/0022-3697\(90\)90021-7](https://doi.org/10.1016/0022-3697(90)90021-7)
- Yin W, Shi T, Yan Y (2014) Unusual defect physics in $\text{CH}_3\text{NH}_3\text{PbI}_3$ perovskite solar cell absorber. *Appl Phys Lett* 104(6):063903. <https://doi.org/10.1063/1.4864778>
- You J, Hong Z, Yang Y (2014) Low-temperature solution-processed perovskite solar cells with high efficiency and

flexibility. ACS Nano 8(2):1674–1680. <https://doi.org/10.1021/nn406020d>

Zhao K, Munir R, Yan B, Yang Y, Kim T, Amassian A (2015) Solution-processed inorganic copper(I) thiocyanate

(CuSCN) hole transporting layers for efficient p–i–n perovskite solar cells. J Mater Chem A 3(41):20554–20559. <https://doi.org/10.1039/C5TA04028K>